Transaction B: Mechanical Engineering
Vol. 16, No. 5, pp. 425–439

SCIENTIA IRANICA

A New Method in Two Phase Flow Modeling of a Non-Uniform Grid

A. Bohluly[1], S.M. Borghei[1] and M.H. Saidi[2,*]

Abstract. *In this paper, a two dimensional numerical model for two phase flow is presented. For interface tracking, the FGVT-VOF (Fine Grid Volume Tracking-Volume Of Fluid) method is selected. For momentum advection, an improved approach is used. In this scheme, a volume tracking step is coupled with steps of computations for the advection of momentum. A Reynolds stress algebraic equation has been implemented in the algorithm of turbulent modeling. Standard test cases are used for the verification of interface tracking and hydrodynamic modeling in laminar and turbulent conditions. The test results show that this methodology can be used in different applications of two-phase flow modeling.*

Keywords: *Two phase flow; Non-uniform grid; Volume tracking; Volume of fluid.*

INTRODUCTION

In the numerical computation of immiscible multifluid problems with a large density variation such as gas-liquid interfaces, special considerations are needed. This includes the accurate representation of the interface separating the fluids, the accuracy and robustness of surface forces representation and the accessibility to a strong methodology for spatial and large density variation problems.

In several basic numerical methods designed for simulating gas-liquid flows, the liquid flow is calculated and the dynamics of the gas phase is neglected [1]. There are cases in which the gas phase is calculated separately. The most well-known is the Marker And Cell (MAC) method [2] in which Lagrangian marker particles are advected with the local fluid velocity with their distribution, determining the instantaneous fluid configuration.

However, in the general case of the rise of a gas bubble in a liquid, the gas phase dynamics cannot be neglected. Thus, the problem arises from an incompressible fluid with large fluid distortions and large density variations. For this reason, in more advanced research work, the domain of the two phase is solved together.

One of the most important problems for multifluid modeling is simulation of the flow interface. The known basic methodologies for this object are "front tracking or surface tracking" and "surface capturing".

Surface-tracking explicitly treats the interface as a discontinuity. Usually it is specified by an ordered set of marker points, connected by an interpolation curve [3]. The marker points are advected explicitly by a Lagrangian method for interface tracking. In some front-tracking methods, the interface is represented by an interface grid [4].

Surface-capturing or volume-tracking methods are implicit with respect to the interface. In these methods, multiphase distribution is described by using a special function. The best known volume-tracking method presented by Hirt and Nicholls [1] is the Volume Of Fluid (VOF). Another common volume tracking method is the level set approach, according to Osher and Sethian [5]. The level set method is improved by mixing it with other methods and has been widely used in recent works [6-10]. Both methods handle the complicated interfaces including their merging and break up more easily than the surface-tracking methods. An exhaustive review of volume-tracking methods is presented by Rider and Kothe [11].

Various techniques are proposed for VOF in order to maintain a well defined interface within the volume

1. *Department of Civil Engineering, Sharif University of Technology, Tehran, P.O. Box 11155-9313, Iran.*
2. *School of Mechanical Engineering, Sharif University of Technology, Tehran, P.O. Box 11155-9567, Iran.*
*. *Corresponding author. E-mail: saman@sharif.edu*

Received 14 May 2008; received in revised form 7 September 2008; accepted 1 November 2008

fraction framework. These fall into the categories of line techniques, the donor-acceptor formulation and higher order differencing schemes. There are also some new approaches with higher accuracy than in the VOF method. For example, Aulisa et al. [12] have developed a VOF method mixed with moveable particles on interfaces that increases the accuracy of estimation of the interface position. However, in some tests, these methods are not practical and the estimation of some important parameters such as density or viscosity is very difficult in them. Youngs [13] gives a useful refinement to the Simple Line Interface Calculation (SLIC) method with the use of oblique lines to approximate the interface in a cell. Ashgriz & Poo [14] improved the SLIC with their Flux Line-segment model for Advection and Interface Reconstruction (FLAIR) using line-segments on the cell faces.

Youngs' second-order-accurate 2D method [13] is the most popular Piecewise Linear Interface Calculation (PLIC) method. The volume-tracking algorithm of Rudman [15] develops the concept of Zalesak's flux corrected transport without interface reconstruction. The method is intensively tested against SLIC, Hirt-Nichols VOF and Youngs' method. Rudman [16] presented Fine Grid Volume Tracking (FGVT) which is a simple but highly accurate approach of the Young method. In this method, for the front capturing method, a finer grid is used.

Most two phase flow modeling is developed with a laminar assumption, but in some hydraulic conditions of a two phase flow, a turbulent condition is present. There are limited studies relevant to modeling turbulent interfacial flows using RANS and/or a large-eddy simulation (LES) in the Eulerian formulation. Between recent works, Shirani et al. used RANS equations for turbulent multi-fluid flow modeling [17].

In this paper, the FGVT-VOF method is selected for simulation of the interface, since it is a very useful method for estimation of equivalent densities and viscosities, and some spatial works are undertaken to increase the accuracy of the advection of momentum. For flow field computations, a fractional step method is used in Reynolds-Averaged Navier-Stokes (RANS) equations. Advection terms of the flow field equations are solved, coupled with a front capturing step. For turbulent modeling, a realizable k-e model has been implemented using a FGVT front capturing model with a non-uniform grid. Implementation of turbulent models under separate flow conditions needs more attention in comparison with single phase conditions.

GOVERNING EQUATIONS

The governing equation for a multiphase flow with a density varying interface is given by the time-dependent RANS equation which can be written in the following form:

$$\frac{\partial C}{\partial t} + \nabla.(\mathbf{u}C) = 0, \tag{1}$$

$$\nabla \mathbf{u} = 0, \tag{2}$$

$$\frac{\partial \rho \mathbf{u}}{\partial t} + \nabla.(\rho \mathbf{u}\mathbf{u}) + \nabla.P = \rho \mathbf{g} + \mathbf{F}_s + \nabla.\left[\mu\left(\nabla.\mathbf{u} + \nabla.\mathbf{u}^T\right)\right], \tag{3}$$

where C is a fractional volume function of the liquid phase (also named a color function), P is the pressure, $\mathbf{u}(u, v)$ is the velocity vector, $\mathbf{g}(g_x, g_y)$ is a vector pointing in the direction of gravity and $\mathbf{F}_s$ is the surface force arising from interfacial effects. The fractional volume function, C, is advected with the local velocity, $\mathbf{u}(u, v)$, by Equation 1. Also, ρ and μ are the density and fluid viscosity under laminar conditions, respectively. In general, for turbulent flow, the eddy viscosity must be added to the laminar viscosity. In multifluid modeling, the density and viscosity are obtained as Equations 4 and 5. In these equations, subscripts 1 and 2 indicate first and second fluids.

$$\rho = C.\rho_1 + (1 - C).\rho_2, \tag{4}$$

$$\mu = C.\mu_1 + (1 - C).\mu_2. \tag{5}$$

In this paper, it is shown that by using the FGVT algorithm, these parameters can be estimated with higher accuracy.

NUMERICAL METHODS

Two phase flow equations are solved in four main steps on a non-uniform grid by a fractional step method. First, the interface is captured by the FGVT technique which is proposed by Rudman [15,16], being a variant of the VOF volume tracking method. In the present study, the FGVT method is implemented into the non-uniform grid and coupled with the advection of momentum. At the second and third steps, the effects of viscosity and body forces are encompassed in the results, respectively. At the fourth step, by the combination of momentum and continuity equations, final pressures and velocities are solved. This methodology is described briefly as follows:

Step 1: Advections of color function (or density) and momentum with the coupled method.

Step 2: Diffusion and effect of viscosity and Reynolds stresses.

Step 3: Effect of body forces are implemented.

Step 4: Pressure and velocity are computed.

DETAILS OF NUMERICAL METHODS

Staggered Grid

For this model, a non-uniform staggered grid is considered as shown in Figure 1. In this type of grid, three types of position are validated as the centers, corners and faces of control volumes.

In this grid, pressure as a scaler variable is located at the center of the cell, densities are located in the faces, viscosities are located at the centers and corners. Vertical and horizontal components of velocities are located on the faces of the cell. The position of the density is very important and effective in two phase flow modeling. It is shown that by using the FGVT algoritm for the colour function advection solution, the high accuracy computations of densities and viscosities are possible in real positions.

The variation of spatial steps in non-uniform grid needs more attention for protection against any excessive error due to this variation.

Interface Reconstruction and Advection of Color Function

As shown in the 1st step of the two-fluid simulation, the interface must be captured by advection of the color function in the flow field. In the common volume of fluid approach, the distribution of phases is represented by volume fraction $C_{i,j}$ of the liquid phase in cell (i, j). The PLIC (Youngs') method uniquely defines the interface in each cell with $0 < C < 1$ by a slope segment which is perpendicular to a given normal, $\mathbf{n}$, to the interface $(n = \nabla.C)$. The main idea of interface construction and advected fluxes of color function is shown in Figure 2 in a control volume.

According to the Youngs' method, the interface normal $(\mathbf{n})$ is initially calculated at each corner of the cells as the gradient of the color function. In this scheme, components of $\mathbf{n}$ are computed by neighboring cells for a non-uniform grid as follows:

$$\begin{aligned}\mathbf{n}_{i+\frac{1}{2},j+\frac{1}{2}} =&[(C_{i+1,j+1} - C_{i,j+1})\Delta y_j \\ &+(C_{i+1,j} - C_{i,j})\Delta y_{j+1}]/ \\ &((\Delta y_j + \Delta y_{j+1}).\Delta x_{i+\frac{1}{2}})\mathbf{i} \\ &+[(C_{i+1,j+1} - C_{i+1,j})\Delta x_i \\ &+(C_{i,j+1} - C_{i,j})\Delta x_{i+1}]/ \\ &((\Delta x_i + \Delta x_{i+1}).\Delta y_{j+\frac{1}{2}})\mathbf{j}. \qquad (6)\end{aligned}$$

The cell-centered normal is calculated by averaging these corner normals.

$$\mathbf{n}_{i,j} = \frac{1}{4}(\mathbf{n}_{i+\frac{1}{2},j+\frac{1}{2}} + \mathbf{n}_{i-\frac{1}{2},j+\frac{1}{2}} + \mathbf{n}_{i+\frac{1}{2},j-\frac{1}{2}} + \mathbf{n}_{i-\frac{1}{2},j-\frac{1}{2}}). \qquad (7)$$

At each time step, after constructing the interface, the flux of the color function is computed by the scheme that is shown in Figure 2. The color function in the new time step is calculated by the FCT-VOF method [15]. At the beginning, set $\Delta V^n_{i,j} = \Delta x_i.\Delta y_j$, then for the x-sweep of the mesh, the following calculations should be set down:

$$\widetilde{C}_{i,j} = C^n_{i,j}\Delta V^n_{i,j} - (F^x_{i+\frac{1}{2},j}F^x_{i-\frac{1}{2},j}),$$

$$\Delta V^{n+\frac{1}{2}}_{i,j} = \Delta V^n_{i,j} - \Delta t\Delta y(u_{i+\frac{1}{2},j} - u_{i-\frac{1}{2},j}),$$

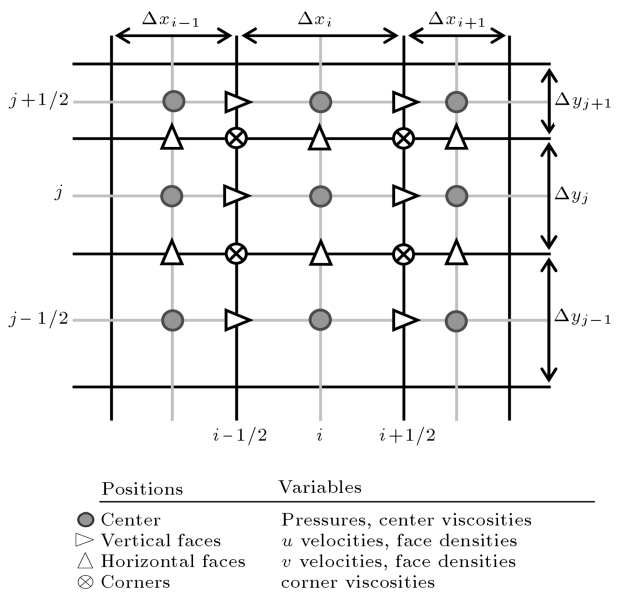

Figure 1. Staggered grid and types of positions and variables in non-uniform grid.

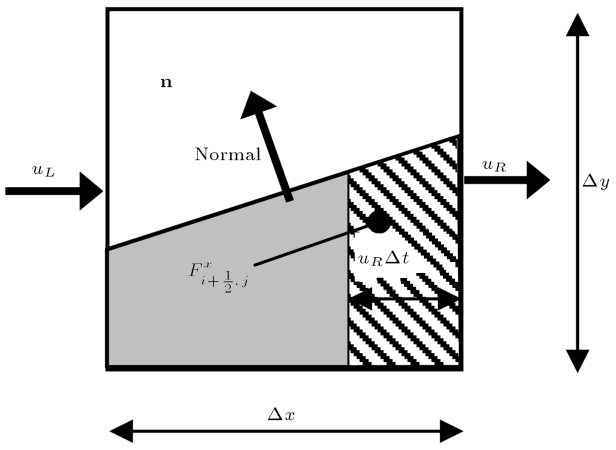

Figure 2. Linear interface construction and advected flux from right face of control volume.

$$C_{i,j}^{n+\frac{1}{2}} = \tilde{C}_{i,j}/\Delta V_{i,j}^{n+\frac{1}{2}}. \quad (8)$$

The y-sweep is calculated similarly. After these two direction sweeps, ΔV should be set again equal to $\Delta x.\Delta y$.

For surface tracking with higher resolution, Rudman [16] proposed the FGVT method. In this method, surface tracking is solved on a grid with half the size of a hydrodynamic grid. This methodology leads to higher accuracy in interface tracking, higher accuracy in density estimation in the face of cells and superior accuracy in the advection of momentum. In Figure 3, the refined grid and new numbering in the FGVT method are shown. In this scheme, each main cell is divided into 4 equal fine cells. Each fine cell has a parameter as color function $c_{i,j}$. In the non-uniform grid, the size of the fine grid is obtained as follows:

$$\Delta x_{2i} = \Delta x_{2i+1} = \frac{1}{2}\Delta x_i,$$

$$\Delta y_{2j} = \Delta x_{2j+1} = \frac{1}{2}\Delta y_j. \quad (9)$$

Since in the fine grid approach there are no parameters such as velocities for volume tracking computation, these parameters must be obtained by interpolation from the coarse grid. In this interpolation, the main attention must be paid to mass conservation. Thus, a simple interpolation is selected for velocities on a fine grid given by Equation 10. This method is also illustrated in Figure 4.

$$(u_{2i+\frac{1}{2},2j})_{\mathrm{FG}} = u_{i+\frac{1}{2},j},$$

$$(u_{2i-\frac{1}{2},2j})_{\mathrm{FG}} = 0.5(u_{i+\frac{1}{2},j} + u_{i-\frac{1}{2},j}). \quad (10)$$

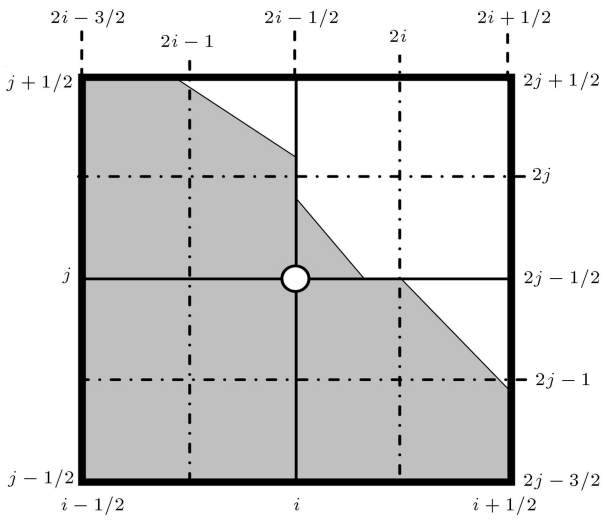

Figure 3. FGVT refined grid and usage of new numbering of fine cells.

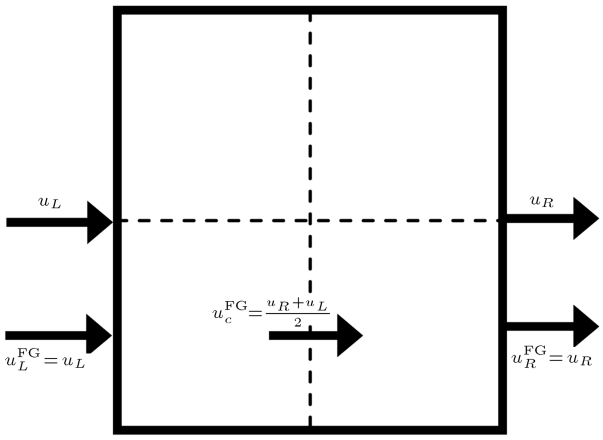

Figure 4. Velocities of a coarse grid cell (solid line) and fine grid cells (dashed line).

Using the color function in the fine grid, some parameters can be solved easily as follows:

$$\rho_{i+\frac{1}{2},j} = 0.5((\rho_{2i,2j} + \rho_{2i,2j-1})\Delta x_i + (\rho_{2i+1,2j} + \rho_{2i+1,2j-1})\Delta x_{i+1})/(\Delta x_i + \Delta x_{i+1}). \quad (11)$$

At the first step after computation of middle color function c^* in the fine grid, it is easy to compute ρ^* in the vertical and horizontal faces of the cells.

Advection of Momentum

One of the major problems in two-fluid modeling is the high density variation at the interface of the fluids. This large density variation makes difficulties for momentum conservations. An additional consideration is that reasonable estimates of flux densities must be made to ensure that momentum fluxes are consistent with mass fluxes.

For this purpose, a second order scheme is used for solution of the momentum advection as follows:

$$\frac{(\rho\mathbf{u})^* - (\rho\mathbf{u})^n}{\Delta t} + \nabla.(\rho\mathbf{u}\mathbf{u}) = 0. \quad (12)$$

An assumption, with good arguments for two-fluid modeling, is made which asserts that although density and hence momentum may be discontinuous across an interface, the velocity field varies smoothly. Due to this discontinuity, the use of high order standard differencing techniques for momentum advection will yield unstable solutions and rapidly destroy the solution, since the Taylor expansion of density is not valid in the neighborhood of the discontinuity.

In recent work, momentum advection is based on the fully multidimensional Zalesak Flux Corrected Transport algorithm (ZFCT) with two significant differences [16]:

1. The calculation of densities and momentum fluxes at the faces of the control volume,
2. The min:max values used in the flux limiter.

For computation of momentum fluxes in an x direction at the 1st step of advection, two types of control volume must be considered for solving Equations 13 and 14.

$$\frac{(\rho u)^* - (\rho u)^n}{\Delta t} + \nabla.(\rho u u) = 0, \tag{13}$$

$$\frac{(\rho v)^* - (\rho v)^n}{\Delta t} + \nabla.(\rho v u) = 0. \tag{14}$$

In Figure 5a, the control volume for Equation 13 is shown. For solving $(\rho u)^*$, the value of $(\rho v)^n$ and the flux of (ρu)that crosses the vertical faces of the control volume must be known. However, $(\rho u)^n$ is known from the last computations or initial conditions. As shown in Figure 5, for high accuracy computation of the momentum flux (hatched area), a good estimate of velocity and density in the hatched area must be known. In a standard MAC algorithm, these densities are obtained using linear or bilinear averages of nearby C-values and Equation 4. In FGVT, an estimate of the average density of the fluid crossing each side of a momentum control volume can be made using the information obtained from the advection of c-values on the fine grid. Considering the x-momentum

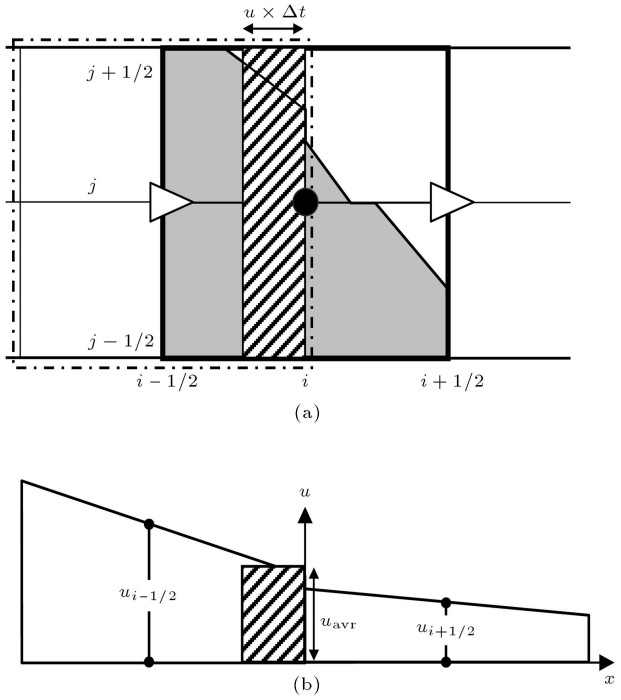

Figure 5. (a) Control volume of momentum of ρu in x direction (dash-dotted line), flux of momentum crossing the vertical face of the control volume (hatched area); (b) linear distribution of u.

control volume centered on $(i-1/2, j)$ and shown in Figure 5, the averaged density of x-momentum flux ρ_m is computed by $F^x_{2i-0.5,2j}$ and $F^x_{2i-0.5,2j-1}$ using Equation 15, which are fluxes of the advected color function in the fine grid. It should be mentioned that F^x_m is the mean void fraction of the fluid crossing the face, i, of a momentum control volume in a time step, as shown in Figure 5.

$$\rho_m = (F^x_m.\rho_1 + (1 - F^x_m).\rho_2),$$

$$F^x_m = \frac{F^x_{2i-\frac{1}{2},2j} + F^x_{2i-\frac{1}{2},2j-1}}{u_{i,j}.\Delta t.\Delta y_j}, \tag{15}$$

2nd order accuracy is used for good estimation of the velocity of the fluid being fluxed across the face of the control volume. In this method, a linear distribution for u velocity is assumed for the upwind control volume, as shown in Figure 5, and is computed by the following equation:

$$u = u_{i-\frac{1}{2}} + s_{i-\frac{1}{2}}.(x - x_{i-\frac{1}{2}}),$$

$$s_{i-\frac{1}{2}} = \frac{u^n_{i+\frac{1}{2},j} - u^n_{i-\frac{3}{2},j}}{\Delta x_{i-1} + \Delta x_i}. \tag{16}$$

By this distribution, the averaged velocity of the x-momentum flux is computed as follows:

$$u_{\text{avr}} = u_{i-\frac{1}{2}} + 0.5(\Delta x_{i-\frac{1}{2}} - u_{i,j}\Delta t)s_{i-\frac{1}{2}} \quad \text{if } u_{i,j} > 0,$$

$$u_{i,j} = 0.5(u_{i+\frac{1}{2},j} + u_{i-\frac{1}{2},j}). \tag{17}$$

The computed u and u_{avr} from the above equations are used in x-momentum computations as;

$$(\rho u)^*_{i-\frac{1}{2}} = (\rho u)^n_{i-\frac{1}{2}} - (\text{flux}^{\rho ux}_i - \text{flux}^{\rho ux}_{i-1})/ (\Delta x_{i-\frac{1}{2}}\Delta y_j), \tag{18}$$

$$\text{flux}^{\rho ux}_i = \rho_m.u_{\text{avr}}.u_{i,j}\Delta t.\Delta y_j. \tag{19}$$

The same methodology as above is used for solving Equation 14. In Figure 6, the control volume of the y-momentum advected by horizontal velocities is shown. This control volume is around the v-velocity position. At this step, the averaged density of the crossing flux is computed by Equation 20, and the flux is computed by Equation 21:

$$\rho_m = (F^x_m.\rho_1 + (1 - F^x_m).\rho_2),$$

$$F^x_m = \frac{F^x_{2i+\frac{1}{2},2j} + F^x_{2i+\frac{1}{2},2j+1}}{u_{i+\frac{1}{2}}.\Delta t.\Delta y_{j+\frac{1}{2}}}, \tag{20}$$

$$\text{flux}^{\rho vx}_{i+\frac{1}{2},j+\frac{1}{2}} = \rho_m.v_{\text{avr}}.u_{i+\frac{1}{2}}, j + \frac{1}{2}.\Delta t.\Delta y_{j+\frac{1}{2}}, \tag{21}$$

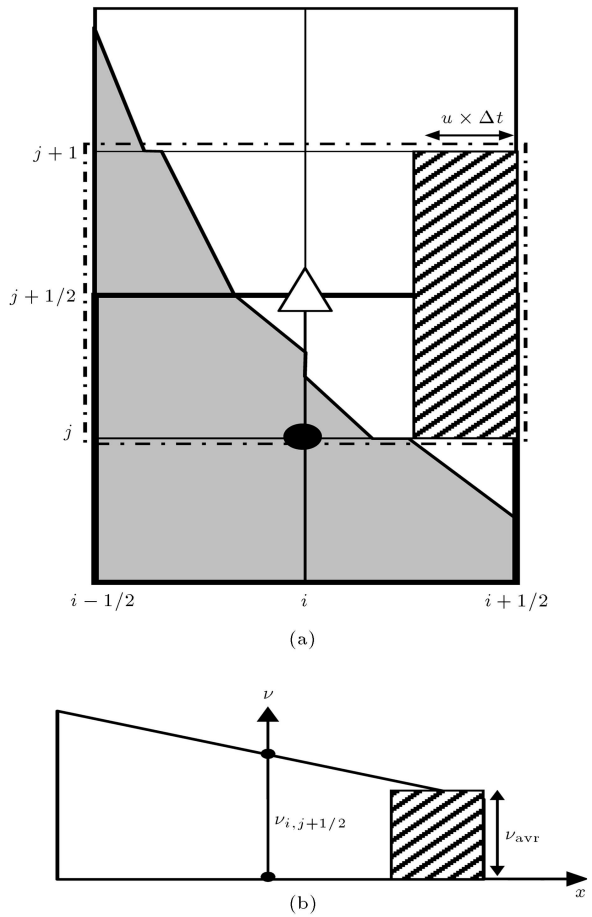

Figure 6. (a) Control volume of momentum of ρv in x direction (dash-dotted line), flux of momentum crossing the vertical face of the control volume (hatched area); and (b) linear distribution of v.

where the averaged v-velocity is computed from Equation 17 and $u_{i+\frac{1}{2},j+\frac{1}{2}}$ is obtained by the linear averaging of two u-velocities in $(i+1/2, j)$ and $(i+1/2, j+1)$ positions.

In the Rudman method [16] for higher-order accuracy, flux limiting is used. Once low- and high-order fluxes have been estimated, anti-diffusive fluxes are calculated and limited in a similar way to the fully multidimensional Zalesak procedure. In the Rudman method, for higher-order flux computation, the averaged velocity in the flux area is computed on vertical faces. However, in this paper, the velocity is obtained in the middle of the flux by assuming a linear variation of velocity. For advection of the color function and momentum by v-velocities, the above steps are repeated by proportional control volumes.

Diffusion by Viscosity

In the 2nd step of the main methodology, as used in this paper, the Reynolds stresses must affect the momentum equation. The effect of Reynolds stresses is given by the following:

$$\frac{(\rho u)^{***} - (\rho u)^{**}}{\partial t} = \frac{\partial}{\partial x}\left(\mu \frac{\partial u}{\partial x}\right) + \frac{\partial}{\partial y}\left(\mu \frac{\partial u}{\partial y}\right). \quad (22)$$

Figure 7 helps to define the numerical solution of Equation 22. In this figure, the best position of equivalent viscosity is shown by multiplied circles in cell corners and filled circles at the center of the cells.

The required position of equivalent viscosity is also given in the following equation:

$$\frac{((\rho u)^{***} - (\rho u)^{**})_{i+\frac{1}{2},j}}{\partial t} =$$
$$\frac{1}{\Delta x_{i+\frac{1}{2}}}\left(\mu_{i+1,j}\frac{u_{i+\frac{3}{2},j} - u_{i+\frac{1}{2},j}}{\Delta x_{i+1}} - \mu_{i,j}\frac{u_{i+\frac{1}{2},j} - u_{i-\frac{1}{2},j}}{\Delta x_i}\right)$$
$$+\frac{1}{\Delta y_j}\left(\mu_{i+\frac{1}{2},j+\frac{1}{2}}\frac{u_{i+\frac{1}{2},j+1} - u_{i+\frac{1}{2},j}}{\Delta y_{j+\frac{1}{2}}} - \mu_{i+\frac{1}{2},j-\frac{1}{2}}\frac{u_{i+\frac{1}{2},j} - u_{i+\frac{1}{2},j-1}}{\Delta y_{j-\frac{1}{2}}}\right). \quad (23)$$

For elimination of averaging, using the FGVT algorithm, the laminar (and eddy) viscosities are computed in both positions. By the implicit Crank-Nicolson method, diffusion equations are solved in the x and y-momentum. After the diffusion steps u^{**} and v^{**} are updated as u^{***} and v^{***}, respectively.

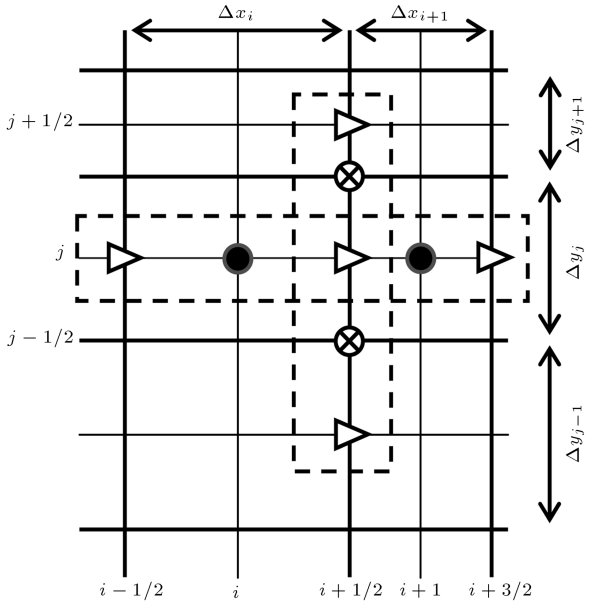

Figure 7. Local grid for Reynolds stresses computation and location of viscosities.

Laminar and Turbulent Viscosity

To use the model under both laminar and turbulent conditions, an equivalent viscosity as $\mu = \mu_l + \mu_t$ is used in the final formulation where μ_l and μ_t are laminar and turbulent viscosities, respectively.

Under high Reynolds conditions, a realizable Reynolds stress algebraic equation model [18] is used for the Reynolds stress term. The latter model has significantly improved the predictive capability of $k-\varepsilon$ based models especially for flows involving strong shear layers. The equations for these models are:

$$\frac{\partial k}{\partial t} + \mathbf{u}.\nabla k = \nabla.\left[\frac{1}{\rho}(\mu_l + \mu_t/\sigma_k)\nabla k\right] + \frac{1}{\rho}(G_k + G_b - \varepsilon), \tag{24}$$

$$\frac{\partial \varepsilon}{\partial t} + \mathbf{u}.\nabla \varepsilon = \nabla.\left[\frac{1}{\rho}(\mu_l + \mu_t/\sigma_\varepsilon)\nabla \varepsilon\right] + \frac{1}{\rho}\left(C_{1\varepsilon}\frac{\varepsilon}{k}(G_k + C_{3\varepsilon}G_b)\right) - C_{2\varepsilon}\frac{\varepsilon^2}{k}, \tag{25}$$

where, eddy viscosity is computed from:

$$\mu_t = \rho C_\mu \frac{k^2}{\varepsilon}, \tag{26}$$

where k and ε are turbulent kinetic energy and dissipation rate, respectively, the turbulent Prandtl numbers for k and ε values are $\sigma_k = 1$, $\sigma_\varepsilon = 1.3$, and the coefficient values are $C_{1\varepsilon} = 1.44$ and $C_{2\varepsilon} = 1.92$. Also, G_k is the generation of turbulent kinetic energy due to mean velocity gradients and G_b is the generation of turbulent kinetic energy due to buoyancy.

$$G_k = -\rho\overline{u_i' u_j'}\frac{\partial u_j}{\partial x_i} = -\rho\left(\overline{u'u'}\frac{\partial u}{\partial x} + \overline{u'v'}\left(\frac{\partial u}{\partial y} + \frac{\partial v}{\partial x}\right) + \overline{v'v'}\frac{\partial v}{\partial y}\right),$$

$$S = \sqrt{G_k/\mu_t}, \tag{27}$$

$$G_b = \frac{\mu_t}{\rho P_{rt}}\left(-g_x\frac{\partial \rho}{\partial x} - g_y\frac{\partial \rho}{\partial y}\right), \quad P_{rt} = 0.85. \tag{28}$$

In the realizable model, estimation of the Reynolds stress tensor, $\overline{u_i' u_j'}$, can be written as:

$$\overline{u_i' u_j'} = \frac{2}{3}k\delta_{ij} - C_\mu(k^2/\varepsilon)2S_{ij} + 2C_2(k^3/\varepsilon^2)(-S_{ik}\Omega_{kj} + S_{kj}\Omega_{ik}), \tag{29}$$

where:

$$S_{ij} = \frac{1}{2}\left(\frac{\partial u_i}{\partial x_j} + \frac{\partial u_j}{\partial x_i}\right) - \frac{1}{3}\frac{\partial u_k}{\partial x_k}\delta_{ij}, \tag{30}$$

$$\Omega_{ij} = \frac{1}{2}\left(\frac{\partial u_i}{\partial x_j} - \frac{\partial u_j}{\partial x_i}\right). \tag{31}$$

In the standard $k-\varepsilon$ model $C_\mu = 0.09$ and $C_2 = 0$. However, for the algebraic model, these coefficients are:

$$C_\mu = \frac{1}{6.5 + A(Uk/\varepsilon)},$$

$$C_2 = \frac{\sqrt{1 - 9S_{ij}S_{ij}C_\mu\left(k/\varepsilon\right)^2}}{1 + 6\left(\sqrt{S_{ij}S_{ij}}\left(k/\varepsilon\right)\sqrt{\Omega_{ij}\Omega_{ij}}\left(k/\varepsilon\right)\right)}, \tag{32}$$

$$U = \sqrt{S_{ij}S_{ij} + \Omega_{ij}\Omega_{ij}},$$

$$A = \sqrt{6}\cos\left[\frac{1}{3}\arccos\left(\sqrt{6}W\right)\right],$$

$$W = \frac{S_{ij}S_{jk}S_{ki}}{\left(S_{ij}S_{ij}\right)^{\frac{3}{2}}}. \tag{33}$$

For computation of the buoyancy effect in Equation 29, a spatial method is used:

$$G_b = \frac{2\mu_t}{P_{rt}}\left(-g_x\frac{\rho_{i+\frac{1}{2},j} - \rho_{i-\frac{1}{2},j}}{\Delta x\left(\rho_{i+\frac{1}{2},j} + \rho_{i-\frac{1}{2},j}\right)} - g_y\frac{\rho_{i,j+\frac{1}{2}} - \rho_{i,j-\frac{1}{2}}}{\Delta y\left(\rho_{i,j+\frac{1}{2}} + \rho_{i,j-\frac{1}{2}}\right)}\right). \tag{34}$$

The third constant of the $k-\varepsilon$ model is computed by $C_{3\varepsilon} = \tanh|v_g/u_g|$ where v_g is the flow velocity parallel to the gravitational vector and u_g is perpendicular to the gravitational vector [19].

Turbulent conditions in separated flow are affected strongly by the interface. The interface limits the vorticity sizes in the vicinity of the separation surface between high and low density fluid. These limitations are due to some additional forces such as surface tension and buoyancy.

For computation of laminar viscosity in the center and corner of cells, initially, cell-centered viscosities in the fine grid are computed using the computed color function as follows:

$$\mu_{l,2i,2j}^{\mathrm{FG}} = c_{2i,2j}^{n+1}\mu_1 + \left(1 - c_{2i,2j}^{n+1}\right)\mu_2, \tag{35}$$

where $\mu_{l,2i,2j}^{\mathrm{FG}}$ is the equivalent laminar viscosity in cell centers of the fine grid. Rudman has proposed a harmonic averaging for equilibrium viscosity in the

cell-corner, given by Equation 36. While this equation is only used in the x-momentum equation; for the y-momentum Equation 37 is used.

$$\mu^x_{i+\frac{1}{2},j+\frac{1}{2}} = \left(\mu^{\rm FG}_{2i,2j} + \mu^{\rm FG}_{2i+1,2j}\right).\left(\mu^{\rm FG}_{2i,2j+1} + \mu^{\rm FG}_{2i+1,2j+1}\right)/ \left(\mu^{\rm FG}_{2i,2j} + \mu^{\rm FG}_{2i+1,2j} + \mu^{\rm FG}_{2i,2j+1} + \mu^{\rm FG}_{2i+1,2j+1}\right), \quad (36)$$

$$\mu^y_{i+\frac{1}{2},j+\frac{1}{2}} = \left(\mu^{\rm FG}_{2i,2j} + \mu^{\rm FG}_{2i,2j+1}\right).\left(\mu^{\rm FG}_{2i+1,2j} + \mu^{\rm FG}_{2i+1,2j+1}\right)/ \left(\mu^{\rm FG}_{2i,2j} + \mu^{\rm FG}_{2i+1,2j} + \mu^{\rm FG}_{2i,2j+1} + \mu^{\rm FG}_{2i+1,2j+1}\right). \quad (37)$$

The above averaging is affected by the variation of spatial steps and by the weight of the fine grid cell area in the non-uniform grid. Equation 38 introduces computation of the cell-center laminar viscosity.

$$\mu_{l,i,j} = \frac{1}{4}(\mu^{\rm FG}_{l,2i-1,2j-1} + \mu^{\rm FG}_{l,2i,2j} + \mu^{\rm FG}_{l,2i,2j-1} + \mu^{\rm FG}_{l,2i-1,2j}). \quad (38)$$

Considering Effects of the Surface Tension and Gravity

In our formulations, body forces, including the effects of gravity accelerations and surface tensions, are considered. At this step, velocities in momentum equations are updated as:

$$u^s = u^{***} + g_x\Delta t + \frac{1}{\rho_{i+\frac{1}{2},j}} F_{x,i+\frac{1}{2},j}\Delta t,$$

$$v^s = v^{***} + g_y\Delta t + \frac{1}{\rho_{i,j+\frac{1}{2}}} F_{y,i,j+\frac{1}{2}}\Delta t, \quad (39)$$

where F_x and F_y are components of the $\mathbf{F}_s$ surface force arising from interfacial effects.

The Pressure Calculation, based on the Interface Location (PCIL) method, presented by Shirani et al. [20], is used for surface tension. This method is based on calculation of the pressure force at each interfacial cell face using the exact pressure due to the portion of the cell face that is occupied by each fluid. In the PCIL method, interface forces are computed as:

$$\mathbf{F}_s = H\sigma\kappa\delta_s\mathbf{n} = H\sigma\kappa\mathbf{n}\frac{|\nabla\tilde{C}|}{[C]}, \quad (40)$$

where σ is the equivalent surface tension coefficient, κ is the interface curvature, $\mathbf{n}$ is the unit normal vector of the interface and H is a non-dimensional parameter that denotes the location of the interface at the cell side ($H_R = l_R/\Delta y$ as in Figure 8). The sign of $\sim$ (or tilda) denotes a filtered or smoothed value and the square brackets denote the difference between the maximum and the minimum values of the function inside the brackets.

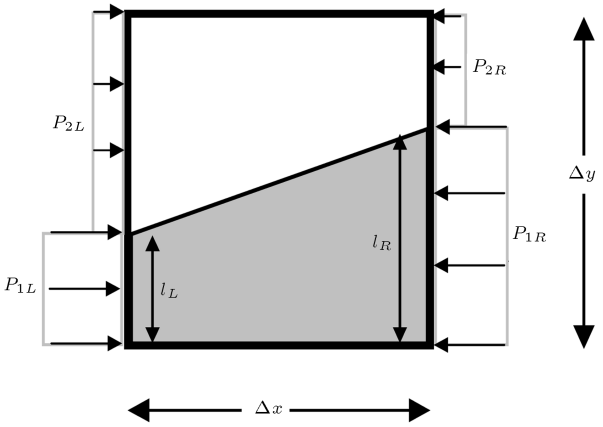

Figure 8. An interface cell with cell face pressures along the x-axis.

In a turbulent flow condition, due to the existence of a fluctuation of velocities and pressure, the behavior of the surface tension is different. Shirani et. al. [17] proposed a new method for obtaining this term under turbulent conditions. They show that the unresolved high-frequency small-scale fluctuations of curvature in a turbulent flow can be represented by increasing the mean curvature, $\overline{\kappa}$, by a factor of $\sqrt{\mu_t/\mu}$, due to turbulence effects with the proper coefficient. It shows that the surface tension force in a turbulent flow is increased by a factor of $\sqrt{\mu_t/\mu}$.

This methodology is used for general conditions of laminar and turbulent flows as follows:

$$\sigma = \sigma_0 + \sigma_t = \sigma_0\left(1 + C_p\sqrt{\mu_t/\mu}\right), \quad (41)$$

where σ_0 is the molecular surface tension coefficient, σ_t is the turbulent surface tension coefficient and C_p is the model constant to be determined due to calibration.

Pressure and Velocity Computing

At this step, continuity and remained momentum equations are discretized as:

$$\nabla.\mathbf{u} = 0 \Rightarrow \Delta y.\left(u^{n+1}_{i+\frac{1}{2},j} - u^{n+1}_{i-\frac{1}{2},j}\right) + \Delta x.\left(v^{n+1}_{i,j+\frac{1}{2}} - v^{n+1}_{i,j+\frac{1}{2}}\right) = 0, \quad (42)$$

$$\frac{\partial\rho\mathbf{u}}{\partial t} + \nabla.P = 0 \Rightarrow$$

$$\begin{cases} \rho_{i+\frac{1}{2},j}\left(u^{n+1}_{i+\frac{1}{2},j} - u^{s}_{i+\frac{1}{2},j}\right) = \Delta t.\left(P^{n+1}_{i+1,j} - P^{n+1}_{i,j}\right)/\Delta x \\ \rho_{i,j+\frac{1}{2}}\left(v^{n+1}_{i,j+\frac{1}{2}} - v^{s}_{i,j+\frac{1}{2}}\right) = \Delta t.\left(P^{n+1}_{i,j+1} - P^{n+1}_{i,j}\right)/\Delta y \end{cases} \quad (43)$$

By overlaying Equation 43 by Equation 42, the discretized Poisson equation is obtained.

The Poisson equation can be written as $\mathbf{A} \times \mathbf{P}^{n+1} = \mathbf{B}$. The system of linear equations is solved directly by the LU (Lower/Upper triangular decomposition) method, which is optimized for a bounded matrix, and the pressures at the new time steps are obtained. After computing the pressure using Equation 43, new velocities in the new time step are obtained.

RESULTS

In order to check the validity of the numerical model, a number of test cases have been considered. These include verification tests for the volume tracking method and two-phase flow models.

Interface Tracking by VOF in a Convergent-Divergent Channel

In this test case, a channel is considered where the center line coincides with the x-axis of the coordinate system and function $f(x)$ specifies the distance between the channel wall and the center line. The velocity field is derived from the assumption that the component, u, parallel to the center line has a parabolic profile at every cross-section of the channel. The only solenoidal velocity field (u, v) having a parabolic profile of u at every cross section of the channel is given by:

$$u = \left(1 - \left(\frac{y}{f(x)}\right)^2\right) \frac{1}{f(x)},$$

$$v = \left(1 - \left(\frac{y}{f(x)}\right)^2\right) \frac{y}{(f(x))^2} \frac{d}{dx} f(x), \tag{44}$$

and the channel profile is given by:

$$f(x) = 1 - a \exp\left[-\frac{1}{2}\left(\frac{x}{b}\right)^2\right],$$

$$a = 0.75, \quad b = 0.5. \tag{45}$$

The computational domain is the rectangle $[-2.5, 2.5] \times [-1.0, 1.0]$ divided into 250×100 computational cells, implying square computational cells of side length $\Delta x = \Delta y = 0.02$. For the initial condition of the interface, a bubble is located at the point $(1.95, 0)$ and its radius is 0.5.

The final state is considered at time $t = 2020\ \Delta t$. The time step, Δt, corresponds to the Courant number, $C = 0.3$ or $\Delta t = 0.001465$.

The results of FGVT-VOF are shown in Figure 9 for the initial $t = 0$, $t = 1220\ \Delta t$ and $t = 2020\ \Delta t$. Figure 10 shows the result of the test procedure when applied to the following different interface tracking methods:

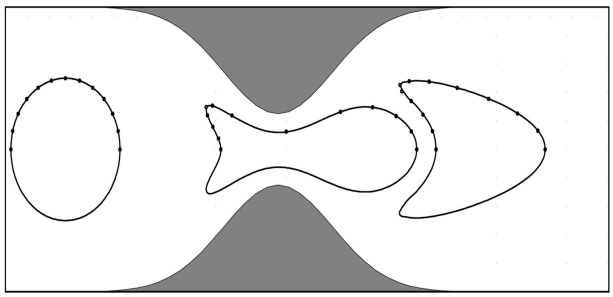

Figure 9. Results of convergent-divergent channel modeling by FGVT-VOF method; circles are exact solutions, solid lines are FGVT solutions.

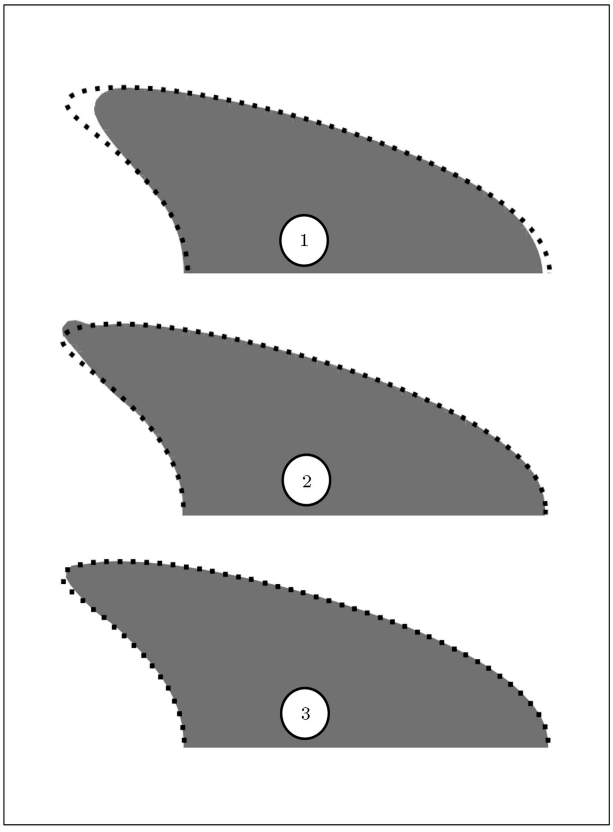

Figure 10. Results of convergent-divergent channel modeling by differen methods. (1) Level Set method; (2) Unsplit PLIC VOF; and (3) FGVT VOF method.

1. Level Set [21],
2. Unsplit PLIC-VOF [22],
3. FGVT-VOF method used in this paper.

Results show that VOF methods have superior volume conservation properties, but are liable to develop small-scale topological irregularities like the outward bend of the two "fine tips" in the final state. However, using the finer grid in the FGVT method reduces these irregularities.

Lock Exchange Test Case

The lock exchange flow is a well-known test case to verify the modeling of density currents. The name of this test case originates from the practical engineering problem concerning the intrusion of a salt water wedge under fresh water when a lock gate is opened at the mouth of a fresh water channel leading to the sea. This test case is selected for verification of a two phase flow model. Two incompressible fluids with slightly different density confined in a rectangular basin with impermeable walls, are initially divided by a very thin wall as shown in Figure 11. Under the initial condition, the left half of the domain is filled by fluid of a higher density and the right half by fluid of a lower density.

Under equilibrium conditions, the velocity of the density current can be estimated from energy conservation considerations as:

$$U_c = \sqrt{0.5 \frac{\rho_2 - \rho_1}{\rho_2 + \rho_1} gH}. \tag{46}$$

The model configuration is set to match that of Jankowski [23] with channel length $L = 30$ m and depth $H = 4$ m. The horizontal and vertical resolutions are $\Delta x = 0.2$ m, $\Delta y = 0.2$ m and CFL $= 0.1$. Initially, the left and right halves of the basin are occupied by water of density $\rho_2 = 1000.722$ kg/m^3 and $\rho_1 = 999.972$ kg/m^3, respectively.

In Figure 12, the results of a two phase flow modeling and an ordinary density current simulation for a lock exchange problem are shown. In Figure 13, the time series current speed in the middle of a channel at points at the surface and the bottom are shown. Figure 12 shows agreement between these two types of modeling, but two phase modeling is the same as the analytical solution otherwise ordinary solutions have some diffusion errors. Also, in Figure 13, it can be seen that two phase flow modeling is fully symmetric. These results show that the model can be used for density current simulations if immiscibility is considered in phenomena.

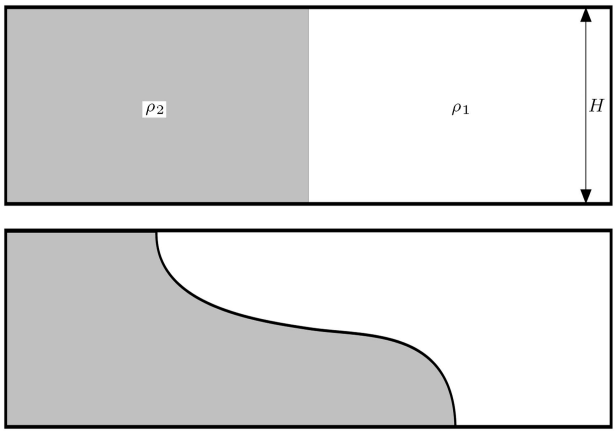

Figure 11. Lock exchange problem.

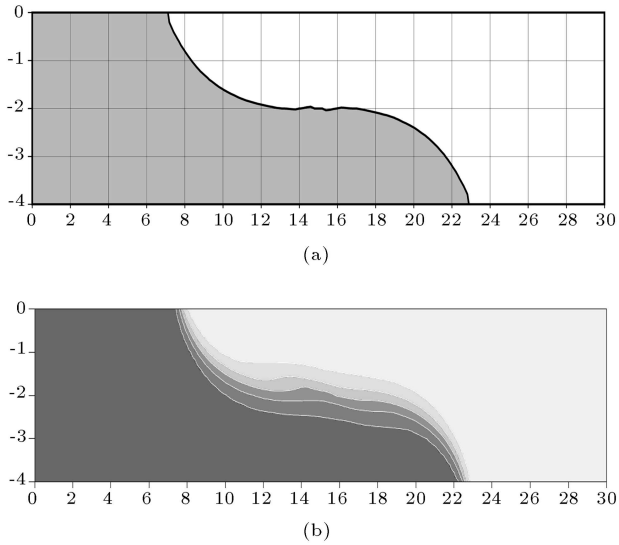

Figure 12. The results of lock exchange problem after 100 sec. (a) Simulated by two phase flow modeling in present work; and (b) Ordinary density current simulation [23].

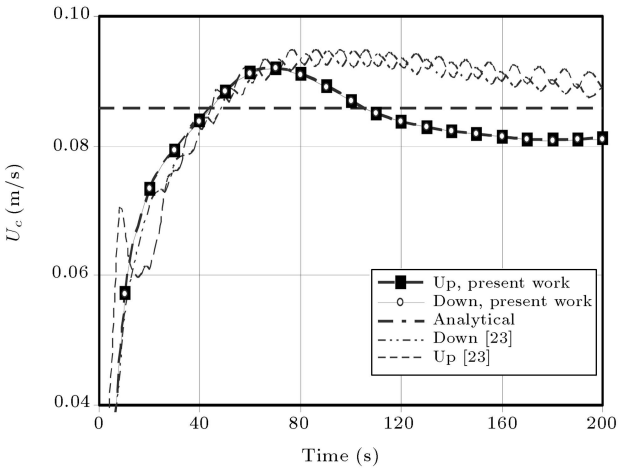

Figure 13. The lock exchange flow wedge speed (density current) time series for points at surface and bottom (up and down) in middle of the basin.

Dam Break Modeling

For two-phase flow modeling with high density variations, the experimental data of Martin and Moyce are used [24]. Figure 14 shows the initial conditions of a column of water (a) and the time evolution (b) of a dambreak test case. In Figure 15, the numerical results, as a non-dimensional (a) surge front position and (b) height of water column, are compared to the experimental data. Reasonable agreement between the numerical simulation and the experiments is observed, as shown in Figure 15.

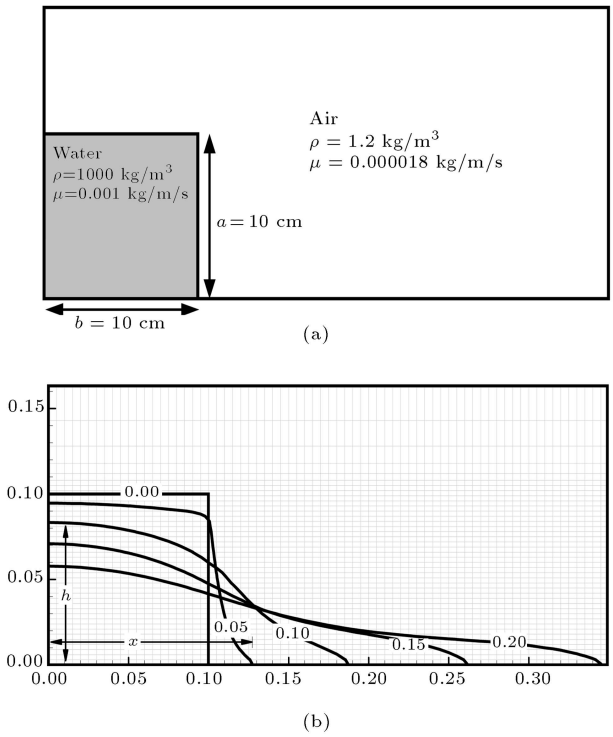

Figure 14. (a) Initial condition for column of water and (b) results of two phase flow modeling at different stages on a non-uniform structured grid for validation of the two phase flow model.

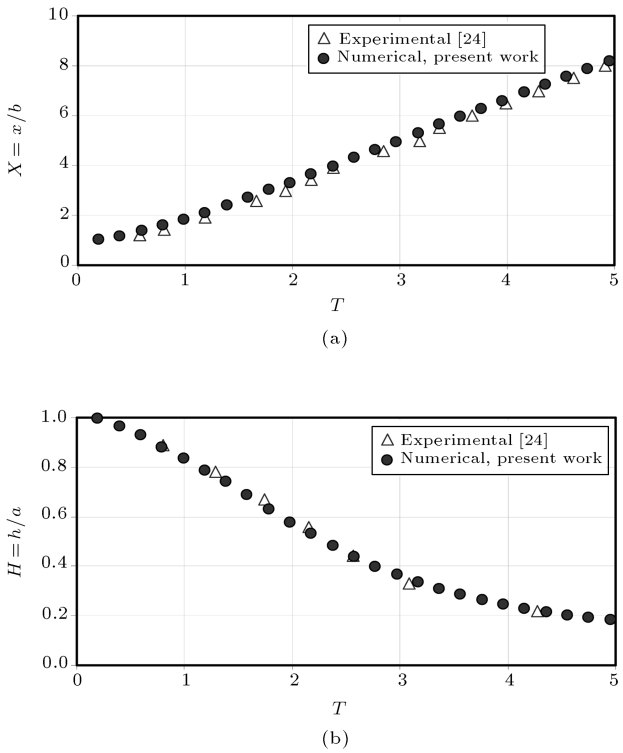

Figure 15. Comparison of non-dimensional results of 2D numerical model with the experimental data [24] at different non-dimensional times. (a) X-surge front position; and (b) H-height of water column collapsing.

Dam Break Modeling with Obstacle

For verification of the capabilities of interface-capturing methods, the dam-break problem with an obstacle is considered as a standard test case for computing free-surface flows. As shown in Figure 16, the barrier holding back the fluid is suddenly removed for the dambreak example. As water flows to the right, it hits an obstacle thus flowing over it and hitting the opposite wall. The confined air escapes upwards as the water falls to the floor on the other side of the obstacle. The initial conditions and dimensions are shown in Figure 16 and the numerical modeling is shown for different time steps in Figure 17. Also, as illustrated in Figure 18, the numerical results are compared well

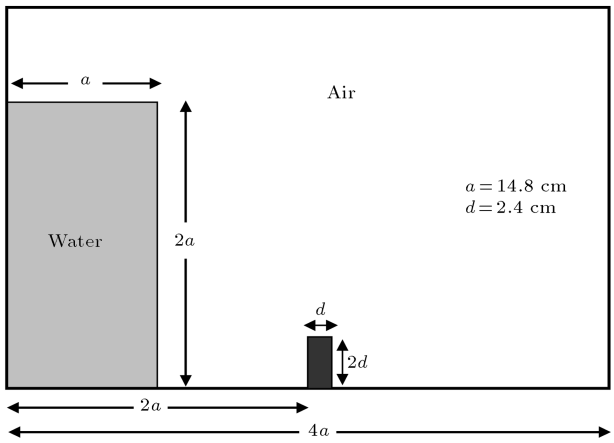

Figure 16. Dimensions and initial condition for dambreak test case with obstacle.

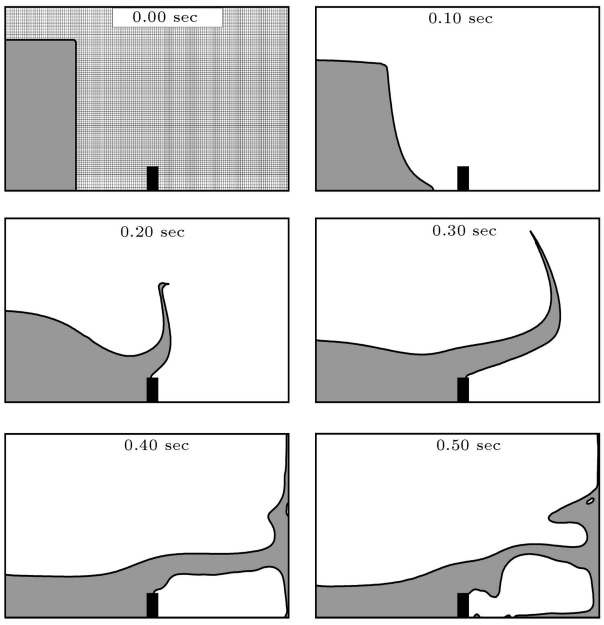

Figure 17. Results of two phase flow modeling at different time steps from 0 to 0.5 sec.

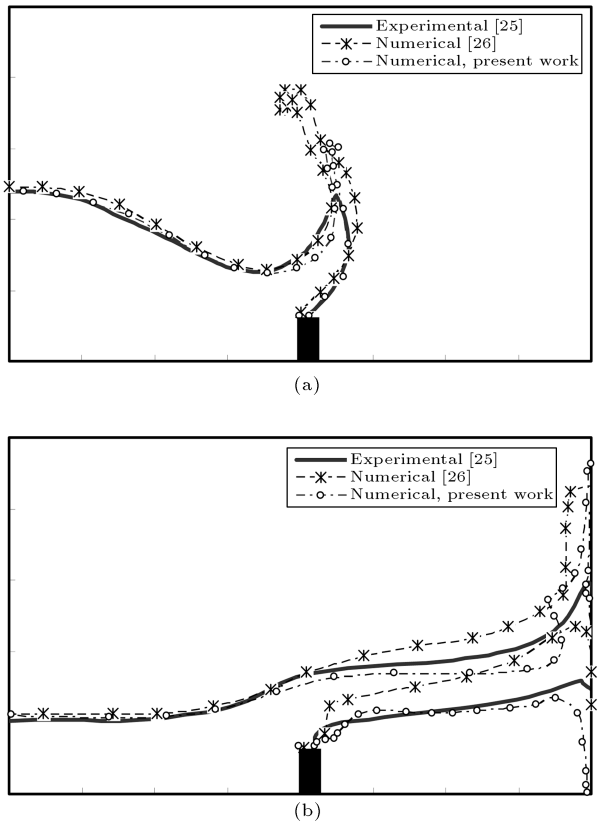

Figure 18. Comparison of results of 2D numerical model with the experimental data of Koshizuka et al. [25] and numerical results of Mujaferija et al. [26] at two stages (a) 0.2 sec. and (b) 0.4 sec.

with the experiments of Koshizuka et al. [25] and the numerical predictions of Muzaferija and Peric [26] at the two time steps of $t_1 = 0.2$ sec and $t_2 = 0.4$ sec after breaking.

Settling Tank

A final test case is selected for verification of the turbulent modeling under a two phase flow condition in which turbulent modeling is undertaken in the inlet region of a rectangular laboratory scale settling tank. The experimental results of this case were presented by Lyn and Rodi [27] and the details of it are shown in Figure 19. Effects of the presence of sediments are not considered. and the average velocity, U, is 1.6 cm/s.

Two types of computational grid with 0.5 × 0.5 and 0.25 × 0.25 cm spatial size are used. In both types of grid, after the recirculation zone, the grid size is increased. The global results of this simulation are shown in Figure 20. In 5 positions, namely at 4, 8, 10, 18, 30 and 40 cm which are shown in Figure 20, the vertical profile of the horizontal velocity is compared with experimental and numerical results. The results of the two types of grid are shown in Figure 21, and are compared with the experimental data of

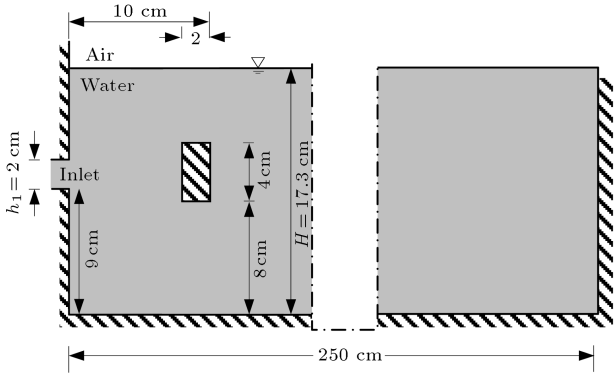

Figure 19. Details of settling tank and deflector.

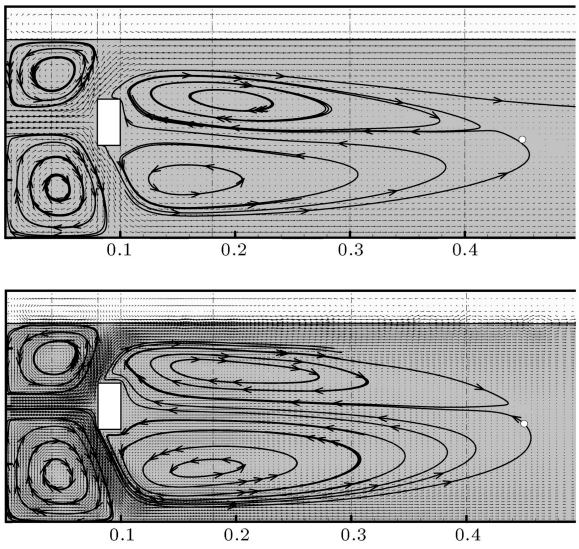

Figure 20. Results of settling tank modeling by turbulence two phase flow model on two different computational grids 0.5 × 0.5 (top) and 0.25 × 0.25 (down).

Lyn and Rodi [27]. The results show a fairly good agreement with experimental data without considering any specific assumption in the two phase modeling. These types of modeling are usually performed with single phase modeling and for turbulent models with symmetric conditions on a free surface as well.

CONCLUSIONS

In this paper, a numerical model for a two phase flow simulation under general conditions such as laminar and turbulent, is presented. The FGVT method is used for computation of the interface tracking and is coupled with the second order advection solution of momentum equations. Discretization of a second order coupled method without any limiters is presented for momentum advection under high density variation conditions. Equivalent laminar viscosity at two types of position in a computational grid is used. The

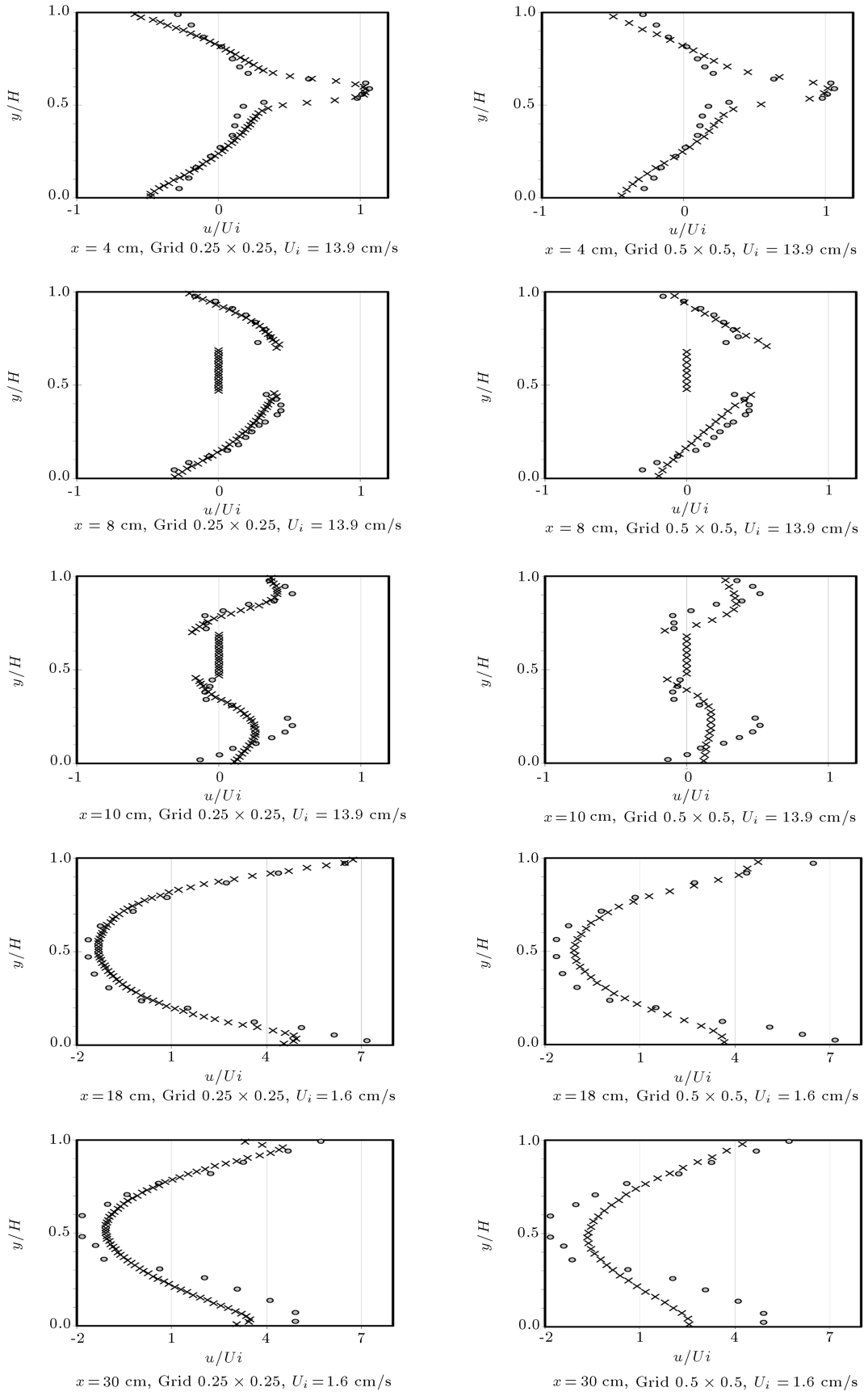

Figure 21. Comparison results of computational modeling with two grid sizes and experimental results [27], in vertical profiles of non-dimensional velocity in settling tank.

$k-\varepsilon$ model is used for turbulent simulation. For the verification of interface tracking one test case is used and for hydrodynamic modeling three test cases are selected, i.e. exchange flow and a dam break with and without obstacles. The results of modeling are tested with analytical or experimental results. All results compare well with other experimental, analytical and numerical results.

NOMENCLATURE

c	volume function of liquid phase in fine grid
C	volume function of liquid phase in main grid
$\text{flux}^{\rho ux}$	flux of momentum of ρu in x direction
F^x	flux of advected colour function in x direction in fin grid
F_m^x	mean void fraction of fluid crossing the velocity control volume
$\mathbf{F_s}$	body forces of surface tension
g_x, g_y	components of acceleration vector in x and y direction
G_k	generation of turbulent kinetic energy
G_b	generation of turbulent kinetic energy due to buoyancy
H	non-dimensional location of the interface at cell side
k	turbulent kinetic energy
$\mathbf{n}$	interface normal
P	pressure
S_{ij}	strain tensor
u, v	local velocity components in x and y direction
u_{avr}	averaged velocity of x-momentum flux

Greek Symbol

$\Delta x, \Delta y$	spatial steps of grid in x and y direction
Δt	time step
ΔV	volume or area of cell
ε	dissipation rate of energy
κ	interface curvature
μ_1, μ_2	fluid viscosity of first and second phase
ρ_1, ρ_2	fluid density of first and second phase
ρ_f	averaged density of x-momentum flux
$\sigma_k, \sigma_\varepsilon$	Prantle numbers for turbulent k and ε
σ	surface tension coefficient

Superscript

n	pesent time step
$n+1$	view time step
s	affected by body forces
$*$	affected by advection in x direction
$**$	affected by advection in y direction
$***$	affected by diffusion
$'$	Reynolds fluctuating part

Subscript

i, j	cell numbering in main grid
$2i, 2j$	cell numbering in fine grid
FG	cine grid
L, R, C	left, right, center
avr	averaged
t	turbulence
l	laminar

REFERENCES

1. Hirt, C.W. and Nichols, B.D. "Volume Of Fluid (VOF) method for the dynamic of free boundaries", *Journal of Computational Physics*, **39**, pp. 201-225 (1981).
2. Harlow, F. and Welch, J. "Numerical calculation of time-dependent viscous incompressible flow of fluid with free surface", *The Physics of Fluids*, **8**(12), pp. 2182-2189 (1965).
3. Popinet, S. and Zaleski, S. "A front-tracking algorithm for accurate representation of surface tension", *International Journal for Numerical Methods in Fluids*, **30**(6), pp. 775-793 (1999).
4. Unverdi, S.H. and Tryggvason, G. "A front-tracking method for viscous, incompressible, multi-fluid flows", *Journal of Computational Physics*, **100**, pp. 25-37 (1992).
5. Osher, S. and Sethian, J.A. "Fronts propagating with curvature-dependent speed: Algorithms based on Hamilton-Jacobi formulations", *Journal of Computational Physics*, **79**(1), pp. 12-49 (1988).
6. Enright, D., Losasso, F. and Fedkiw, R. "A fast and accurate semi-lagrangian particle level set method", *Computers and Structures*, **83**, pp. 479-490 (2005).
7. Sussman, M. "A second order coupled level set and volume-of-fluid method for computing growth and collapse of vapor bubbles", *Journal of Computational Physics*, **187**, pp. 110-136 (2003).
8. Van Der Pijl, S.P., Segal, A. and Vuik, C. "A mass-conservation level-set (MCLS) method for modeling of multiphase flows", *ISSN 1389-6520, Report 03-03 of the Department of Applied Mathematical Analysis*, Delft (2003).
9. Tanguy, S., Menard, T., Berlemont, A. "A level set method for vaporizing two-phase flows", *Journal of Computational Physics*, **221**, pp. 837-853 (2007).
10. Fukagata, K., Kasagi, N., Ua-arayaporn, P. and Himeno, T. "Numerical simulation of gas-liquid two-phase flow and convective heat transfer in a micro

tube", *International Journal of Heat and Fluid Flow*, **28**, pp. 72-82 (2007).

11. Rider, W.J. and Kothe, D.B. "Reconstructing volume tracking", *Journal of Computational Physics*, **141**, pp. 112-152 (1998).
12. Aulisa, E., Manservisi, S. and Scardovelli, R. "A mixed markers and volume-of-fluid method for the reconstruction and advection of interfaces in two-phase and free-boundary flows", *Journal of Computational Physics*, **188**, pp. 611-639 (2003).
13. Youngs, D.L. "Time-dependent multi-material flow with large fluid distortion", in *Numerical Methods for Fluid Dynamics*, edited by Morton, K.W. and Baines, M.J., Academic Press, New York, pp. 273-285 (1982).
14. Ashgriz, N. and Poo, J.Y. "FLAIR: Flux line-segment model for advection and interface reconstruction", *Journal of Computational Physics*, **39**, pp. 201-225 (1991).
15. Rudman, M. "Volume-tracking methods for interfacial flow calculations", *International Journal for Numerical Methods in Fluids*, **24**, pp. 671-691 (1997).
16. Rudman, M. "A volume-tracking method for incompressible multifluid flows with large density variations", *International Journal for Numerical Methods in Fluids*, **28**, pp. 357-378 (1998).
17. Shirani, E., Jafari, A. and Ashgriz, N. "Turbulence models for flows with free surfaces and interfaces", *AIAA Journal*, **44**(7), pp. 1454-1462 (2006).
18. Shih, T.H., Zhu, J. and Lumley, J.L. "A new Reynolds stress algebraic equation model", *Computer Methods in Applied Mechanics and Engineering*, **125**(1), pp. 287-302 (1995).
19. Henkes, R.A.W.M., Van der Flugt, F.F., Hoogendoorn, C.J. et al. "Natural convection flow in a square cavity calculated with low-Reynolds-number turbulence models", *International Journal Heat Mass Transfer*, **34**, pp. 1543-1557 (1991).
20. Shirani, E., Ashgriz, N. and Mostaghimi, J. "Interface pressure calculation based on conservation of momentum for front capturing methods", *Journal of Computational Physics*, **203**, pp. 154-175 (2005).
21. Sussman, M., Almgren, A.S., Bell, J.B. and Colella, M. "An adaptive level set approach for incompressible two-phase flows", *Journal of Computational Physics*, **148**, pp. 81-124 (1999).
22. Meier, M., Yadigaroglu, G. and Andreani, M. "Numerical and experimental study of large steam-air bubbles injected in a water pool", *Nuclear Science and Engineering*, **136**, pp. 363-375 (2000).
23. Jankowski, J.A. "A non-hydrostatic model for free surface flows", Ph.D. Thesis, University of Hannover (1999).
24. Martin, J.C. and Moyce, W.J. "An experimental study of the collapse of liquid columns on a rigid horizontal plane", *Philosophical Transactions of the Royal Society of London*, **244**, pp. 312-324 (1952).
25. Koshizuka, S., Tamako, H. and Oka, Y. "A particle method for incompressible viscous flow with fluid fragmentation", *Computational Fluid Dynamics Journal*, **4**, pp. 29-46 (1995).
26. Muzaferija, S. and Peric, M. "Computation of free surface flows using interface-tracking and interface-capturing methods", in *Nonlinear Water Wave Interaction*, O. Mahrenholtz, M. Markiewicz, Eds., Chap. 2, pp. 59-100, WIT Press, Southampton (1999).
27. Lyn, D.A. and Rodi, W. "Turbulence measurements in model settling tank", *Journal of Hydraulic Engineering*, **116**(1), pp. 3-21 (1990).